

Satellite mapping of CO emission from forest fires in Northwest America using MOPITT measurements

Jane Liu^{a,*}, James R. Drummond^a, Qinbin Li^b, John C. Gille^c, Daniel C. Ziskin^c

^aDepartment of Physics, University of Toronto, 60 St. George Street, Toronto, Ontario, Canada M5S 1A7

^bJet Propulsion Laboratory, California Institute of Technology, Mail Stop 183-501, 4800 Oak Grove Drive, Pasadena, CA 91109, USA

^cNational Center for Atmospheric Research, P.O. Box 3000, Boulder, CO 80307-300, USA

Received 5 October 2004; received in revised form 28 January 2005; accepted 29 January 2005

Abstract

We present a study on MOPITT (Measurements Of Pollution In The Troposphere) detection of CO emission from large forest fires in the year 2000 in the northwest United States. Fire data used are from the space-borne Advanced Very High Resolution Radiometer (AVHRR) at 1-km resolution. The study shows that MOPITT can reliably detect CO plumes from forest fires whenever there are >30 AVHRR hotspots in a $0.25^\circ \times 0.25^\circ$ grid, which is comparable to the pixel area of MOPITT in the region. The spatial CO pattern during the fire events is found to be consistent with the location and density of AVHRR hotspots and wind direction. While the increase of CO abundance inside the study area is closely correlated to the AVHRR-derived hotspot number in general ($R > 0.75$), the non-linearity of fire emission with fuel consumption is also observed. MOPITT can also capture the temporal variation in CO emission from forest fires through 3-day composites so it may offer an opportunity to enhance our knowledge of temporal fire emission over large areas. The CO emission is quantitatively estimated with a one-box model. The result is compared with a bottom-up approach using surface data including burnt area, biomass density, and fire emission factors. If mean emission factors for the region are used, the bottom-up approach results in total emission estimates which are 10%–50% lower than the MOPITT-based estimate. In spite of the limitations and uncertainties addressed in this study, MOPITT data may provide a useful constraint on uncertain ground-based fire emission estimates.

© 2005 Elsevier Inc. All rights reserved.

Keywords: MOPITT; Fire emission; Carbon monoxide; Remote sensing; Biomass burning; CO pollution; Biosphere-atmosphere interaction

1. Introduction

Carbon monoxide (CO) is an important trace gas in the atmosphere, which plays a significant role in atmospheric chemistry. CO substantially affects the budgets of hydroxyl radicals (OH) and ozone (O₃), two of the most important tropospheric constituents. It is generally agreed that biomass burning accounts for about one quarter of CO emission to the atmosphere with an average of around 600 Mt (1 Mt=10⁹ kg) CO per year (Khalil et al., 1999). The occurrence of biomass burning, the fire sizes, and the fire properties (i.e., smoldering vs. flaming) vary greatly with

time and space. Andreae and Merlet (2001) estimated that mean CO emission from vegetation fires in savanna and tropical forests is 342 Mt CO per year, while the total CO emission for all non-tropical forest fires is 68 Mt CO per year. Although biomass burning in North America is not as predominant as that in savanna and tropical forests, CO emission from vegetation fires considerably impacts air quality on the continent. For example, severe forest fires in Canada in 1995 led to greatly enhanced CO levels in the United States (Wotawa & Trainer, 2000). In addition, the year-to-year biomass burning in this region can vary by a factor of 10 (Amiro et al., 2001; Duncan et al., 2003). The burnt forest area in Canada in 1995 was the largest for the last 40 years and 27 times that in 1978, the year with the lowest burnt area (Amiro et al., 2001).

* Corresponding author. Tel.: +1 416 978 0341; fax: +1 416 978 9805.

E-mail address: jliu@atmosph.physics.utoronto.ca (J. Liu).

Because satellite remote sensing allows consistent, frequent, and extensive data collection at regional and global scales, scientists have explored its use in studying biomass burning and fire emission. Parameters deduced from satellite data include fire counts, burnt area, aerosol index, and biomass density (Ahern et al., 2001; Cooke et al., 1996; Delmas et al., 1991; Dwyer et al., 2000; Fraser et al., 2000; Hsu et al., 1996; Kasischke & French, 1995; Levine, 1991, 1996; Roy et al., 2002; Van der Werf et al., 2003). CO emission from vegetation fires has been indirectly estimated using these parameters from satellite data (Barbosa et al., 1999; Cahoon et al., 1994; Duncan et al., 2003; Heald et al., 2003; Schultz, 2002). In 1981, the first direct space-based measurement of atmospheric CO was made with the Measurement of Air Pollution from Satellites (MAPS) instrument on the shuttle STS-2 flight, and elevated CO from biomass burning was observed in later flights (Connors et al., 1996; Reichle et al., 1986).

Measurements Of Pollution In The Troposphere (MOPITT) is an instrument on board NASA's Terra earth observation system (EOS) satellite, which was launched on December 18, 1999. MOPITT has provided, for the first time, derived CO measurements from space over several years. Since its launch, MOPITT has observed CO enhancement in the atmosphere from biomass burning in various regions around the world (Bremer et al., 2004; Edwards et al., 2002; Lamarque et al., 2003; Liu & Drummond, 2002; Liu et al., 2003a,b). With MOPITT data, spatial and temporal variations of CO emission from biomass burning can be examined directly and independently from other approaches.

Traditionally, CO emission is estimated from ground data on fuel consumption during fire events, the so called "bottom-up" approach, for which knowledge of the burnt area, biomass density, and parameters on emission ratios are prerequisites (Andreae & Merlet, 2001; Hao & Liu, 1994; Seiler & Crutzen, 1980). Since 1997, inversion models have been developed to derive the emission from CO concentration (Bergamaschi et al., 2000; Kasibhatla et al., 2002; Manning et al., 1997), including those with MOPITT CO data (Arellano et al., 2004; Pétron et al., 2004). Large discrepancies between the two approaches are found in some regions. For example, the inversion studies consistently suggest that bottom-up approaches underestimate anthropogenic CO emissions in the northern hemisphere (Arellano et al., 2004).

In the summer of 2000, large forest fires emerged in the northwest of America and enhanced CO plumes were observed in MOPITT imagery (Lamarque et al., 2003; Liu & Drummond, 2002). Lamarque et al. (2003) identified the CO released from the biomass burning and the transportation of the CO originating from the fires to the east of United States. In this study, we correlated the AVHRR (Advanced Very High Resolution Radiometer) fire data with the MOPITT CO data and focused on the following issues that were not addressed in previous studies. First, MOPITT's capability to detect CO emission from forest

fires in relation to fire size was analyzed with our knowledge of average biomass density, emission parameters, and transport speed in North America and assessed with the MOPITT data. Second, the possibility of using MOPITT CO data to improve our knowledge of the temporal variations of fire emissions was investigated with time series of MOPITT CO data and AVHRR fire count data. Third, we explored methods for quantitative assessment of CO emission from biomass burning using MOPITT data: we employed a one-box model to estimate the total fire emission from the study area and compared its magnitude with a "bottom-up" approach. The limitations of MOPITT for detecting and quantifying CO emission from biomass burning are also discussed.

2. Some background information on MOPITT CO data and AVHRR fire count data

2.1. MOPITT CO data

MOPITT is a gas correlation radiometer operating at wavelengths of 4.7 μm and 2.3 μm on the Terra polar orbiting platform at a height of 705 km (Drummond, 1992; Drummond & Mand, 1996). MOPITT has a horizontal resolution of 22 km \times 22 km at nadir and takes about 3 days for near-complete global coverage. MOPITT level 2 data include CO total column and CO mixing ratio at 7 heights (surface, 850, 700, 500, 350, 250, and 150 h Pa).

The methodology of CO retrievals from radiance measurements has been discussed in detail (Deeter et al., 2003; Edwards et al., 1999; Pan et al., 1998). The following points are of particular importance for this paper.

The CO profiles are retrieved using an optimal estimate of the maximum likelihood solution (Pan et al., 1998; Rogers, 2000). With this technique, the retrieved CO profiles depend not only on MOPITT radiance measurements, but also on the a priori CO profile and the averaging kernels. The single a priori CO profile is generated from 525 in-situ profile measurements (Deeter et al., 2003; Fig. 1a) and is used to constrain the solutions because the retrieval problem is ill posed. Fig. 1a provides a general pattern of the CO profile in the troposphere, which contains about 90% of the CO in the atmosphere. The averaging kernels, determined by the a priori error covariance and the retrieval error covariance for each profile, indicate the sensitivity of the retrieved CO to the measurement. A typical set of averaging kernels is shown in Fig. 1b, which suggests that CO retrievals at the surface, 850 hPa, and 700 hPa are most sensitive to the CO around 700 hPa. This illustrates that the MOPITT profile data are highly correlated (Deeter et al., 2003, 2004). The averaging kernels in Fig. 1b also indicate low sensitivity of the retrieved CO to the CO near the surface (the boundary layer). The CO total column is obtained by integrating the CO mixing ratio at 35 heights from the surface to the top of the atmosphere (0.2 hPa).

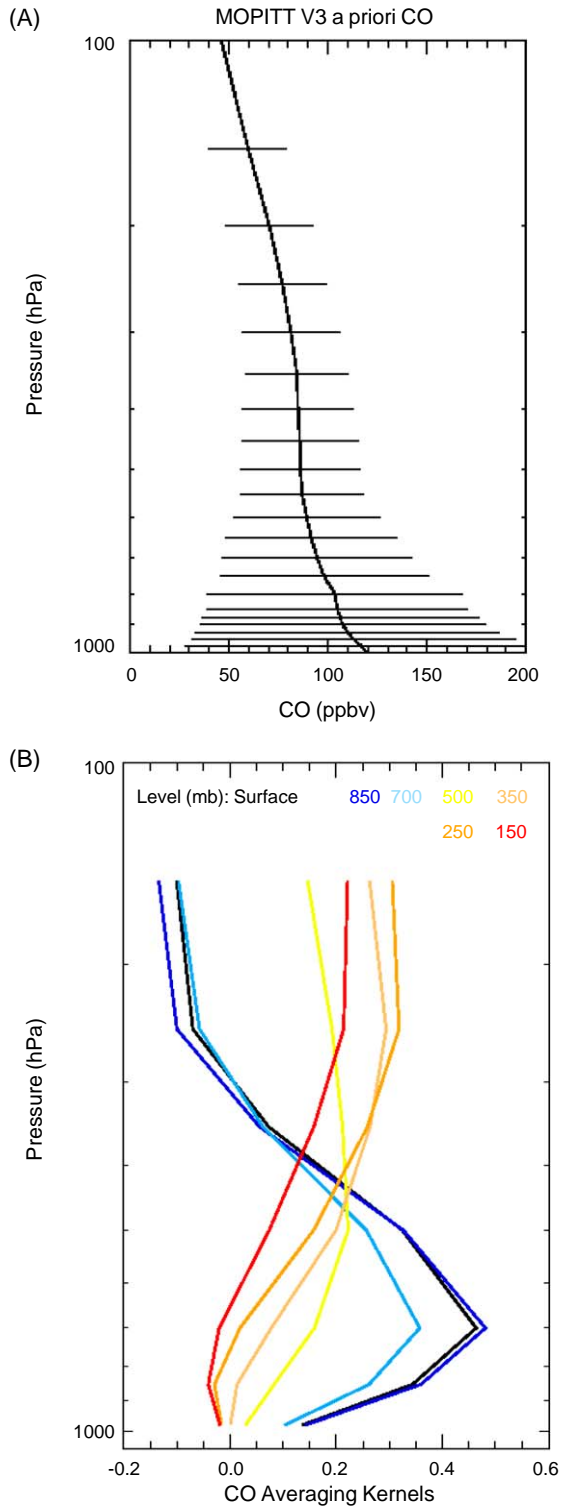


Fig. 1. The global constant a priori (A) and an example set of averaging kernels (B) for MOPITT CO retrieval (after Deeter et al., 2003).

Validation of MOPITT CO data has been performed with various sets of correlative data and good agreement between MOPITT data and in situ aircraft measurement is found (Emmons et al., 2004; Jacob et al., 2003). Emmons et al. (2004) reported an average bias of less than 20 ppbv

for profile data and an average bias of total CO column of $5 \pm 11\%$ from March 2000 to May 2001. These comparisons were performed by convolving the in situ observations with the MOPITT averaging kernel, so the vertical sensitivity of the instrument does not play a role in the comparison.

2.2. AVHRR fire data

The AVHRR instrument has been flown on several NOAA (National Oceanic and Atmospheric Administration) satellites in polar orbit. Because it has a large swath (e.g., 2600 km for that onboard NOAA-14 satellite), AVHRR can provide daily coverage over North America at 1 km resolution. In theory, fires, burning at a temperature of 500–1200 K, emit strong infrared radiation that can be detected by AVHRR's thermal channel 3 (3.7 μm) and channel 4 (10.8 μm). Practically, several fire detection algorithms have been developed (Dwyer et al., 2000; Giglio et al., 1999; Li et al., 2000). A number of limitations are generally associated with the AVHRR fire product. As an optical instrument, AVHRR cannot detect fires under cloudy conditions. It only offers a snapshot of the total number of hotspots during a 24-h period and so it may miss fires with short lifetimes. Small fires (less than $1.0 \times 10^{-3} \text{ km}^2$) may not be detected by some detection algorithms (Giglio et al., 1999). Some bright and hot objects, such as sun-glint over water, barren land, and clouds, may cause false alarms in AVHRR fire data (Li et al., 2003).

3. Study area and data

3.1. Study area

An area (Fig. 2), covering $2.65 \times 10^6 \text{ km}^2$, with a center close to the joint borders of Idaho, Montana, and Wyoming in the United States (108.75° W and 46.25° N) was selected for this study because a series of large fires occurred in the area in the summer of 2000. The extent of the domain was chosen so that it was sufficiently large to contain CO plumes from severe fires in the area. We chose a geographical projection of 0.25° pixel size, close to 22 km (the approximate size of a MOPITT pixel at 40° N latitude) to maximize the use of MOPITT CO horizontal resolution and to be compatible with the projection of wind data for transport calculations. The image size is 70 by 70 pixels and the georeferences of the image are 55° N and 117.5° W for the upper left pixel. The area ratio of a grid cell to a MOPITT pixel is 0.9, 1.1, and 1.3, for the pixels along the latitude at the top (55° N), the middle (42.65° N), and the bottom (37.5° N) of the image, respectively. The central dimensions of the study domain are 1343 km E-W and 1943 km N-S. The time period from July 16 to September 9, 2000 was selected to cover the development

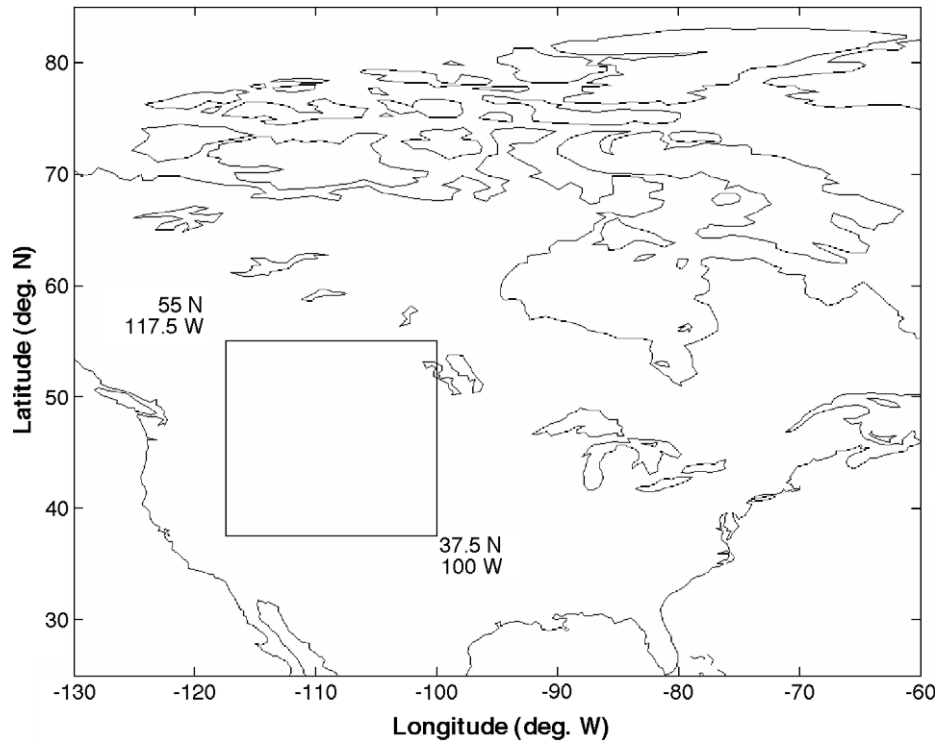


Fig. 2. Location of the study area (boxed) in North America. The domain size is 1943 km in the N–S direction and 1343 km in the E–W direction along the image centre.

of fires in the area since August was the month with the most fires (see Section 4.2). The major land cover types in the area are coniferous forest, grassland and shrubland (Kittel et al., 1996).

The data used for this study include CO (total column and profile) and fire count data from MOPITT and AVHRR, wind data from the National Center for Environment Prediction (NCEP), ground-based burnt area and biomass density from United States Department of Agriculture (USDA) Forest Service. These data are in various formats, usually at global, continent, or regional scales. They were extracted for the study area and were processed to match in space and time. The details are provided as follows.

3.2. CO data

The CO data were derived from the MOPITT Version 3 Level 2 data available at the NASA Langley Distributed Active Archive Center. The original data files contain the total column abundance and the profiles of CO at 7 heights (surface, 850, 700, 500, 350, 250, and 150 hPa), as well as ancillary data including the corresponding location and time along the satellite track in a HDF (Hierarchical Data Format) format on daily basis. Using the location information, CO data were gridded daily at 0.25° resolution. Three-day composites (mean) were made to obtain near-complete coverage (or four-day composites for the last one in months with 31 days). Mean values were taken for pixels having more than one measurement within the time interval.

3.3. Fire count data

Fire data were acquired from the Canada Centre for Remote Sensing (CCRS) in an image format (binary, band sequential (BSQ)). Fires were detected as hotspots with the AVHRR instrument on board NOAA-14 satellite, using the algorithms developed and refined by Li et al. (2000, 2003). The algorithms aimed to maximally eliminate falsely detected fires due to sun-glint and thin clouds. Li et al. (2003) stated that the detection algorithms perform best in forest landcover. In the study area, most fires occurred in forested areas and false alarms were very limited (Li et al., 2003). The images cover North America every day at 1-km resolution in a Lambert conformal conic (LCC) projection (49° and 77° N standard parallels, 95° W meridian). In order to re-project the daily images at 0.25° , an in-house computer program was written based on the map projection methodologies in Snyder (1989). The georeference error for any pixel within North America is within 0.1 km. This assures the accuracy for spatial analysis of the CO and the fire data in this study, especially for Fig. 3. Three-day composites (mean) were made from the daily data.

3.4. Wind data

Daily wind data in longitudinal (U) and latitudinal (V) directions were extracted from the NCEP reanalysis dataset (<http://www.cdc.noaa.gov/cdc/reanalysis/reanalysis.shtml>) (Kalnay et al., 1996) for identifying the wind direction in

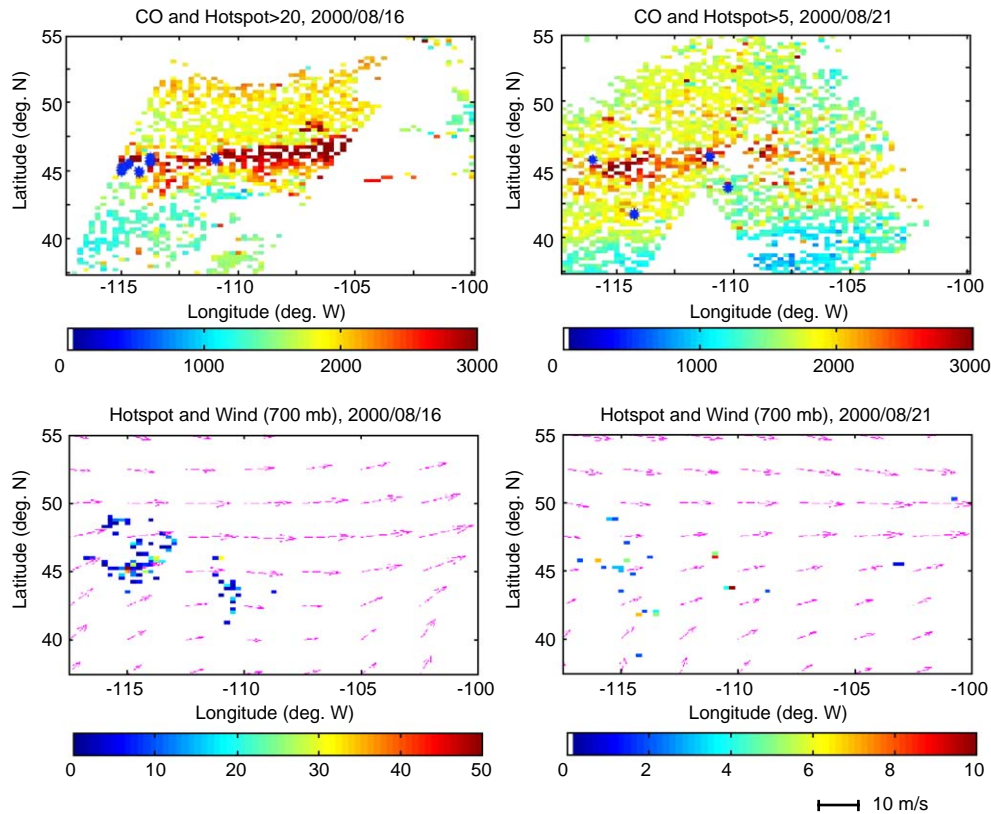


Fig. 3. Images of total column CO (in 10^{15} mol cm^{-2} , top panels), versus the counterpart fire images (bottom panels) on a day with severe fires (August 16) and a day with less severe fires (August 21), as indicated by the total number of hotspots and hotspots per pixel in the fire images (note the different scales in the hotspot images). The locations of relatively large hotspots, with a threshold of 20 for August 16 and 5 for August 21, are marked in blue stars in the corresponding CO images. Daily mean wind fields at 700 mb are overlaid with the corresponding hotspot images (unit and scale for the wind vectors are indicated at the bottom of the figure).

fire event, estimating transport of CO, and generating wind statistics. The raw data have a spatial resolution of 2.5° at 17 heights from 1000 hPa to 10 hPa in the NCL (The NCAR (National Centre for Atmospheric Research) Command Language) format, and only the data at the heights the same as the CO data were used (for 350 hPa, it was taken as the mean of the values at 400 hPa and 300 hPa). Three-day composites (mean) were made from daily values. Using NCL programs, wind data were processed from the NCL format to text format, from the raw digital values to physical variables of interest, and from the globe to the area of interest.

3.5. Ground-based burnt area data

Spatially explicit and spatially implicit data on surface burnt area were acquired for this study. In the former, the spatial pattern of burned area perimeter is described explicitly. The latter only provides statistics (e. g., total) for the burnt area for a region with no information on how the burnt areas are distributed spatially.

The spatially explicit data was generated by the USDA forest Service on basis of surface observations (Li et al., 2003). In the original file, the perimeters of burnt areas were delineated as polygons that were embedded in a geographic information system (GIS) software, ARC/INFO, with a LCC

(Lambert conformal conic) projection (49° and 77° N standard parallels, 95° W meridian). The data were first rasterized into gridded data at 1 km resolution in ARC/INFO and then reprojected to 0.25° resolution. Based on the data, a total of 6937 km^2 was burnt in the study area in 2000.

The spatially implicit (statistical) data on burnt area were from ground reports at the National Interagency Coordination Center (NICC) (<http://www.cidi.org/wildfire/index.html>). This dataset provides monthly ground-reported total burnt area for 11 regions in USA. The study area covered most Northern Rockies and East Great Basin regions, plus a small portion of Rocky Mountain and West Great Basin regions. Therefore, the total burnt area inside the study domain is between the totals in the two regions (Northern Rockies and East Great Basin) and in the four regions (Northern Rockies, East Great Basin, Rocky Mountain, and West Great Basin), an area of between 5569 and 5642 km^2 for forested areas, and between 7525 and 9542 km^2 for all landcover in August 2000.

3.6. Above-ground biomass data

The data on above-ground biomass are obtained from the inventory of USDA Forest Service at <http://www.ncrs.fs.fed.us/4801/tools-data/data>. The data are available only in a

table format on county basis. To make a spatially explicit layer, county boundary data were downloaded from US Census Bureau at <http://www.census.gov/geo/www/cob/co2000.html>. In ARC/INFO, the biomass density was added as an attribute to the county polygons. The biomass density data were merged and generated in a gridded format. The mean aboveground biomass density was 8.46, 7.05, and 6.35 kg m⁻² for Idaho, Montana, and Wyoming, respectively.

3.7. CO emission and burnt area from an earlier study

An estimate of CO emission from an earlier study (Van der Werf et al., 2003) was obtained from University of California at Irvine, at <http://www.ess.uci.edu/~jranders/>, to compare with MOPITT-based emission estimates made in this study. The original data were monthly CO emission per unit area at 1° resolution. The related burnt area data are at the same temporal and spatial resolution.

4. Results and discussion

4.1. Detection of CO plumes

On the basis of our knowledge of biomass density, emission parameters, and transport speed in North America, it is possible for MOPITT, given its horizontal resolution, to detect CO plumes from large forest fires in the continent. The key factors affecting the detection include fire extent, biomass density of burnt areas, and wind field on clear days (in cloudy conditions, MOPITT does not provide valid data). For example, for a 30 km² burnt forest area consuming 50% of the above-ground biomass with a mean above-ground biomass density of 2.6 kg m⁻² for forest in Canada (Amiro et al., 2001), the CO concentration in a MOPITT pixel will be 13.7 times higher than the background level, if we assume that: (1) the emitted CO stays in the air column within a MOPITT pixel; (2) the emission factor for boreal forest is 120 g CO (kg dry matter)⁻¹ (Duncan et al., 2003); (3) the background tropospheric CO is 80 ppbv and evenly mixed through the atmospheric column; and (4) total column of air from the surface to 15 km is 3.15 × 10⁵ moles m⁻² (a typical value for North America in August). Since the mean above-ground forest biomass density in the USA is 7.4 kg m⁻² (USDA Forest Service, 2002) and the emission factor is 107 g CO (kg dry matter)⁻¹ for extratropical forests (Andreae & Merlet, 2001), then the CO concentration in a MOPITT pixel for the USA case will be 34.8 times higher than the background level. However, if the CO is transported into 22 MOPITT pixels 15 hours later at a wind speed of 9 m s⁻¹*, the mean CO in the 22 MOPITT

pixels will be 62% higher than the background for the Canadian case and 157% higher than the background for the USA case. CO emission from small fires or low biomass densities may not be detectable as individual CO plumes, but can contribute to the enhancement of the overall CO level that may be measured by MOPITT.

In the study area, from mid July to early September 2000, a series of fire events occurred. The fire size can be described in terms of the number of hotspots in a grid cell (pixel). Enhanced CO plumes from the fires are visible in the MOPITT CO images when the satellite overpass time matched the burning time. Generally, enhancement of CO in the MOPITT image is evident when the hotspot number was larger than 30 in a 0.25° grid cell. In some cases, the enhancement is perceptible even when the hotspot number was as low as 5. Fig. 3 illustrates this point, showing the CO images on August 16 with severe fires and on August 21 with less severe fires, in conjunction with the corresponding fire images from AVHRR data. Plumes with high CO values are clearly visible on both images. The CO abundance in these plumes had a maximum of about 3.0 × 10¹⁸ molecules cm⁻² on both days, i.e., about twice the background level.

On the CO images, pixels with the fire size greater than a threshold are marked with a star. The threshold is 20 for August 16 and 5 for August 21. Wind fields at 700 hPa are overlaid with the hotspot images. The 700 hPa wind is selected because it usually represents the prevailing wind direction and is approximately within the CO emission injection height of 2–5 km for large forest fires (Lavoué et al., 2000). The elevated CO plumes on the CO images appear to be initiated at places where fire sizes were larger than the respective thresholds near 115° W and 111° W and the plumes were blown along the wind directions on both days. This indicates a good qualitative agreement between the spatial CO distribution and the location and density of fire hotspots accounting for the influence of winds on each day. A land cover map (Kittel et al., 1996) shows that the vegetation where the large hotspots appeared was coniferous forest. The CO image on August 16 is a daytime MOPITT overpass, indicated by the satellite swath from northeast to southwest, while on August 21, it combines both daytime (with a swath from northeast to southwest) and nighttime (with a swath from southeast to northwest) overpasses. The different scale in the two hotspot images suggests that the biomass burning on August 21 was about 3–6 times smaller in density (the number of hotspots per MOPITT pixel) and number of fires. The total number of hotspots in the study area was 92 on August 21, versus 712 on August 16. However, the fires on August 21 emitted a fair amount of CO that resulted in a mean CO abundance of 1.70 × 10¹⁸ molecules cm⁻² in the study area, which is only 10% smaller than that on August 16 (1.92 × 10¹⁸ molecules cm⁻²). We believe the AVHRR captured most fires on August 21 because few clouds appeared in the MOPITT CO image (no many missing values). The large CO plumes on

* The mean wind speeds for North American during the fire season in 2000 based on NCEP/NCAR reanalysis dataset (Kalnay et al., 1996) are: 6.0 m s⁻¹ for 1000 hPa, 7.1 m s⁻¹ for 850 hPa; 8.3 m s⁻¹ for 700 hPa; 11.7 m s⁻¹ for 500 hPa; 18.4 m s⁻¹ for 250 hPa; and 14.0 m s⁻¹ for 150 hPa.

August 21 may possibly be explained by more smoldering fires, as fire phase is another important factor controlling CO emission, besides fuel consumption. Therefore, linearity of CO emission with fuel is warranted only if other influencing factors change little during fire events.

Overlaying daily CO and hotspots images during the entire study period, we visually examined all the cases where at least 20% of CO data were valid in a 10-by-10 pixel window. It is found that MOPITT could detect 30%–100% elevated CO, in comparison with the surrounding background, whenever there were more than 30 hotspots in a 0.25° pixel cell, i.e., a detection rate of 100% (the surrounding background is the CO abundance in the pixels that are not affected by CO emission from fires, usually between 1.4 and 1.5×10^{18} molecules cm^{-2} in the study area and the study period, see Fig. 3). The detection rate decreased to 84% for between 21 and 30 hotspots, to 11% for between 11 and 20 hotspots, and to 3% for less than 11 hotspots. These detection rates were further found to be comparable to a larger domain of the entire Canada and United States in Liu et al. (2003b).

It is difficult to determine the exact burnt area within an AVHRR fire pixel (labeled as hotspot at 1 km resolution) as it depends on fire spread rate. Only when the daily mean fire spread rate is $0.7 \text{ m minute}^{-1}$, i.e., $\sim 1 \text{ km day}^{-1}$, does one hotspot correspond to 1-km^2 burnt area. Over Canadian forests, the peak fire spread rate in a day, averaged from 1971 to 2000, ranges between 0.1 and 6 m minute^{-1} (Natural Resources Canada, 2004). In an effort to reduce the overall uncertainty, we overlaid the AVHRR data at 1 km resolution day by day to examine how often a single pixel was labeled as burnt in a given time. In August 2000 over the study area, on average, a single burnt pixel was observed 1.56 times, and the maximum number was 9 times. This suggests that, on average, one hotspot represents less than 1-km^2 burnt area. It may be safe to use 1-km^2 burnt area per hotspot as an upper limit so that 30 hotspots would cover 6% area of a MOPITT pixel. As 30 hotspots per MOPITT pixel (or the maximum 6% of a MOPITT pixel area to be burnt) produce a detectable CO signal 100% of the time, this may represent a conservative MOPITT detection level for forest fires in North America but this level can be expected to vary with biomass density, fire types (flaming or smoldering), and wind field. In the first paragraph of this section, based on the mean biomass density and the wind speed, we calculate that with a burnt area of 30 km^2 and a period of 15 h, the CO in the plume will be 62% higher than background (no biomass burning) on average for Canadian forest and 157% for USA forest. It appears that this enhancement can be reliably detected by MOPITT. This information could be useful for other studies, for example, for designing a new space-borne CO instrument to investigate vegetation fire emission.

An example of CO variation with height during fire events is displayed in Fig. 4A for August 16 along a cross section between 43° and 49° N (averaged over the

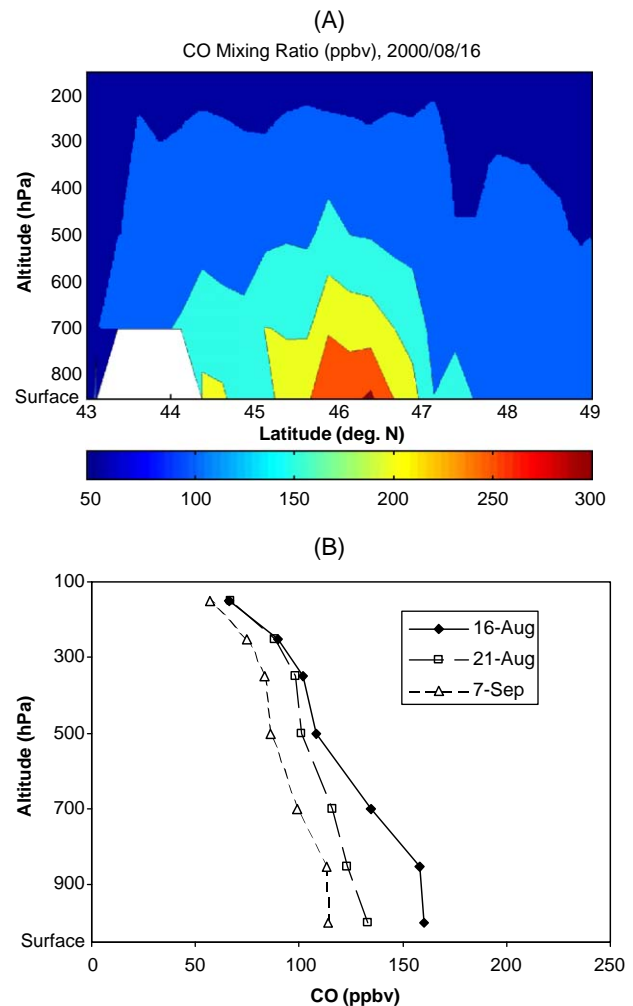


Fig. 4. (A) A latitudinal cross-section of CO with altitude between $43\text{--}49^\circ$ N on August 16, 2000 (see left panels in Fig. 3). White areas indicate missing values. (B) CO profiles on August 16 and August 21, 2000 when 716 and 92 hotspots were counted in the study area, respectively, in comparison with that on September 7 with only 24 hotspots. The value at each pressure level is the mean over the entire image excluding missing values. Note the surface values contain information from the heavily weighted mid-troposphere CO.

longitudes in the study area, see Fig. 3, left panels for the horizontal distributions of CO total column and hotspots on August 16). The CO mixing ratio close to fires was as high as 300 ppbv, in comparison with a CO mixing ratio of 50–100 ppbv in the background. The enhanced CO was transported vertically up to the top of the troposphere and horizontally for a few hundred kilometers. In addition, Fig. 4B shows the comparison of mean vertical CO profiles for different levels of fire severity. The total number of hotspots in the study area was 712 on August 16 and 96 on August 21, compared with 24 on September 7. The enhancement of CO is found to increase with fire severity in almost every profile layer.

As demonstrated in earlier studies, MOPITT has some sensitivity to CO vertical variations associated with tropical deep convection, Asian summer monsoon, and synoptic

weather processes (Deeter et al., 2004; Kar et al., 2004; Liu et al., 2004). Nevertheless, MOPITT’s sensitivity is low to CO in the boundary layer. As a result, the CO values near the surface represent, in large portion, the signal of enhanced CO at mid-troposphere. This implies an underestimate of fire emission if the released CO stays in the boundary layer, which is most likely for the cases with small fires. For large forest fires, the emitted CO usually lofts to upper layers and causes a mixing of CO within troposphere since the heated air is of low density. Occasionally, the convected CO was even observed in the stratosphere (Jost et al., 2004). It should also be noted that the MOPITT instrument does not make an independent measurement at each pressure level. A full interpretation of a profile can be obtained by considering the ‘averaging kernel’, which can be calculated for each profile (Deeter et al., 2003). However, since here we are only considering general trends in highly spatially averaged data, we neglect these effects.

4.2. Temporal variation of CO emission

Because of MOPITT’s revisit time of 2–3 days and the blockage of clouds, there are significant gaps in daily CO images. The percentage of missing data varies from day to day with a mean of 73% and a range of 50%–94% over the period from the July 16 to September 9, 2000. To overcome this problem, three-day composites (or four-day composites for the last one in months with 31 days) were made for both CO and fire images from daily data. Fig. 5 shows the total hotspot counts for each composite for the period, showing the development of the fires from emergence to disappearance in the study area. The total number of hotspots was

~100 in the middle of July, increasing to close to 600 in some composites in August, finally subsiding in early September. The corresponding CO abundance is also shown in Fig. 5, in terms of the total column CO averaged over the CO composite. The CO abundance is closely related to the number of total hotspots most of the time. A noticeable exception is for the period from July 28 to August 3.

To seek reasons for this exception, fire occurrence was checked in a larger domain of 150 × 150 pixels extended from the original image domain by 35 pixels in each direction. The ratio of the total number of hotspots outside the study domain to those inside was 3:1 from July 28 to August 3. Large fires occurred around 35.75° N, 118.25° W, southwest of the study area. Wind field data similar to those in Fig. 3 suggest that some of the CO would have been transported into the study area during the period. This is further confirmed when transported CO is quantitatively calculated in Section 4.3. By contrast, the hotspots inside the study domain from August 22 to 31 were dominant, i. e., 2–4 times more than those outside, and a close relationship between the enhancement of CO and the number of hotspots is observed.

An example of CO and hotspot composites for August 25–27 is displayed in Fig. 6. During August 25–27 with severe fires, the maximum number of hotspots was over 30 in a 0.25° grid cell. The plume of CO expands across the northeast in the image. In 3-day composite images, the percentage of pixels with missing values is reduced from those in the daily images to a mean of 49%. Six-day and nine-day composites are also examined (Fig. 7). Although missing values decrease with more days taken into the composites, the amplitude of temporal variation of CO declines as the time length of the composite exceeds the life cycle of a fire. Nevertheless, the

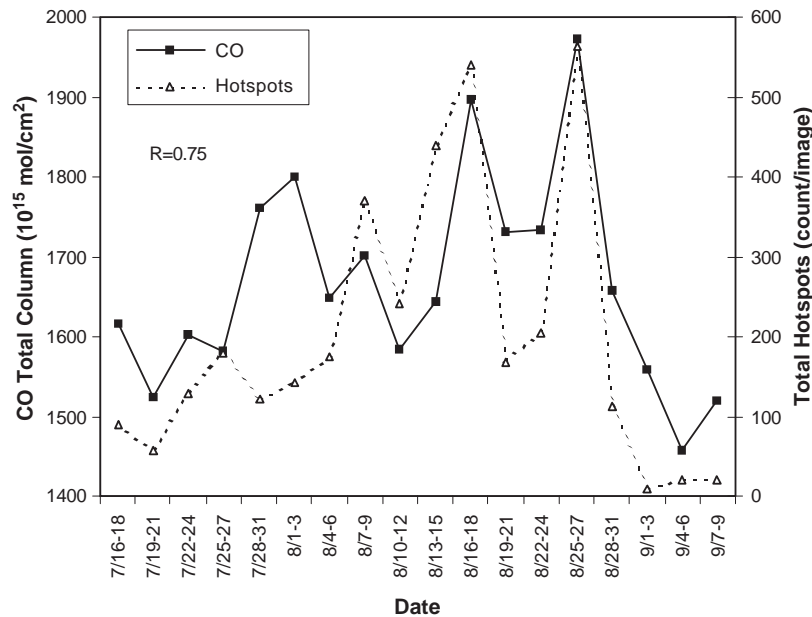


Fig. 5. Temporal variation of fire events and CO abundance from 16–18 July to 7–9 September. The fire events are described in terms of the total number of hotspots for the entire composite image, while the CO abundance is described using total column CO (in 10¹⁵ mol cm⁻²), averaged over the composite image excluding missing pixels. These images are composed of 70 pixels by 70 lines at 0.25° resolution. One hotspot represents fire detection within 1-km² pixel.

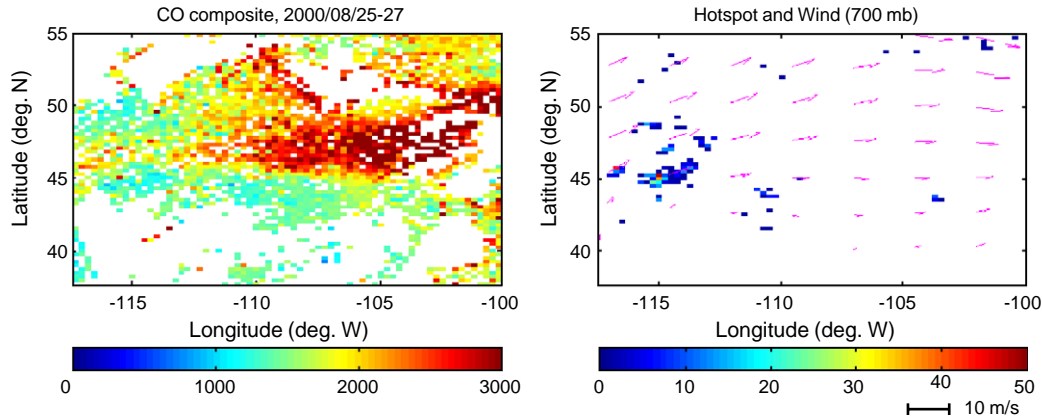


Fig. 6. An example of spatial variation of CO composite image (in 10^{15} mol cm^{-2} , left panel) and hotspot composite image (right panel) for August 25–27, 2000. The hotspot image is overlaid with the wind field at 700 hPa on August 25, 2000 when large fires occurred.

relationship between CO changes and the number of hotspots (the slopes in Fig. 7) in 6-day or 9-day composites is still similar to that in 3-day composites. Considering both temporal variations and data availability, a 3-day composite appears to be a good compromise.

4.3. Magnitude of CO emission

Because MOPITT is not very sensitive to the CO in the boundary layer, it is possible that the retrieved CO values in the boundary layer and its contribution to the CO total column are lower than reality during biomass burning. However, quantitative analysis of MOPITT data may provide a lower bound on CO emission, i.e., at least the portion of CO emitted from biomass burning. In addition, temporal and spatial variations of CO emission and the factors that influence them can be investigated. In this study, we use a one-box model (Jacob, 1999) and primarily MOPITT CO data and NCEP reanalysis wind data to assess

CO emission quantitatively. The study area is considered as a box that is sufficiently large to contain the plumes from fires within a fire event. The horizontal dimensions of the box are ~ 1300 km in E-W direction and ~ 1900 km in N-S direction. The vertical dimension is the whole tropospheric column. Therefore, daily CO emission from biomass burning (CO_{fire} , in kg CO day^{-1}) is equal to the sum of the CO change inside the box, the net CO transported out of the box, net chemical loss (CO_{chem}), less the CO emission from fossil fuel and biofuel (CO_{fuel}). We assume that the deposition loss is negligible, i.e.,

$$\text{CO}_{\text{fire}}(t) = \Delta\text{CO}(t) + [\text{CO}_{\text{out}}(t) - \text{CO}_{\text{in}}(t)] + \text{CO}_{\text{chem}} - \text{CO}_{\text{fuel}} \quad (1)$$

$$\Delta\text{CO}(t) = \left[\sum_{\text{Image}} \text{CO}(x, y, t) - \sum_{\text{Image}} \text{CO}(x, y, t-1) \right] / \Delta t \quad (2)$$

where $\text{CO}(x, y, t)$ is the CO abundance for the pixel (x, y) in the composite image t and $\text{CO}(x, y, t-1)$ is the CO abundance for the same pixel in the previous composite. Δt is the period between the two composites (in days).

The first term on the right side of Eq. (1) can be calculated from Eq. (2). One problem is that there are still some missing values in the composite images like those in Fig. 6, caused by the re-projection of the images (usually small gaps), the satellite track, and clouds (large gaps). The missing CO values were filled with the mean of the nearest data points in all directions weighted inversely by their corresponding distances. The above interpretation method only considers the CO enhancement due to biomass burning. Crawford et al. (2003) reported enhanced CO values in and around frontal clouds. This suggests that high CO could be embedded within clouds mainly due to transport of boundary layer CO to the free troposphere by front lifting, warm conveyor belts (WCB) lifting, or convection in general. Possibly a correction could be made in further studies using daily cloud masks.

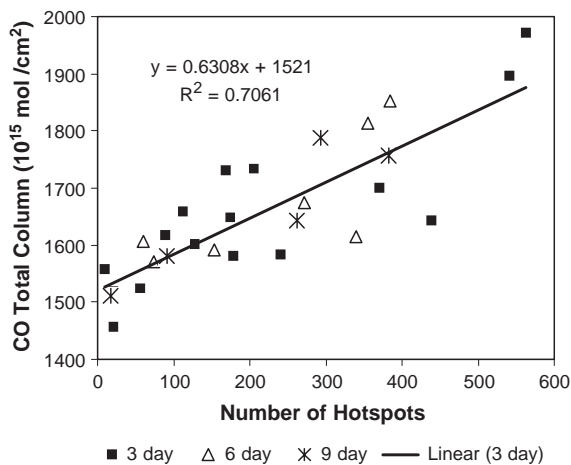


Fig. 7. The enhancement of CO varies with number of hotspots in 3-day, 6-day, and 9-day composites for the study period. Data from 28 July to 3 Aug 2000 are excluded in the calculation because a large amount of CO was transported in from outside. A linear regression with 3-day composite is also given. The slope of the line is 0.63×10^{15} mol CO cm^{-2} hotspot $^{-1}$.

Table 1
Monthly mean of chemical production/loss term in Eq. (1) for July, August, and September 2000, estimated with a 3-D chemical transport model, the GEOS-CHEM model (Bey et al., 2001)

Terms	July (kt CO day ⁻¹)	August (kt CO day ⁻¹)	September (kt CO day ⁻¹)
Production	53	59	24
Loss	45	57	31
Net loss	-8	-2	+7

The 2nd term, the net CO transport, was estimated by assuming that the CO along an edge of the image in a day will transport into or out of the image on the next day, depending on the wind direction. Therefore, we made another set of 3-day/4-day composites at time t' , which is shifted 1 day earlier from the composite at time t for CO and wind at each pressure level. The net transport in each pressure level is a sum of CO flux at the four edges (positive for out-flux and negative for in-flux). The CO flux across the east or the west edge was calculated from the CO mixing ratio at the edge \times longitudinal wind speed (U), while the CO flux across the south or the north edge was calculated from the CO mixing ratio at the edge \times latitudinal wind speed (V). U and V were taken from the means over the study domain to increase stability on wind speed estimation. Finally, total CO transport can be obtained by integrating net transport of CO at each pressure level p , $CO_{transp}(p)$ from:

$$CO(t)_{out} - CO(t)_{in} = \sum_P \Delta P(p) CO_{transp}(p) M_{CO} / (g M_{air}) \quad (3)$$

where p is an index for each pressure level; ΔP is the pressure difference between the levels; g is the acceleration of gravity ($=9.8 \text{ m s}^{-2}$), M_{CO} is the molecular weight of dry

CO ($=28.0 \text{ gram mole}^{-1}$); and M_{air} is the molecular weight of dry air ($=28.97 \text{ gram mole}^{-1}$). The monthly mean (standard deviation) for CO input flux was 1320 (257), 1600 (441), and 2025 (209) kt CO day⁻¹ (1 kt= 10^6 kg) for July, August, and September 2000, respectively, while the monthly mean (standard deviation) for CO output flux was 1347 (256), 1760 (483), 2070 (189) kt CO for July, August, and September 2000, respectively.

The third term is usually much smaller than the other terms during large fire events. Its magnitude was assessed using a global 3-D chemical transport model, the GEOS-CHEM model (Bey et al., 2001). The model was run at 1° by 1° resolution and for year 2000. The CO sources from chemical production considered in the model include the oxidation of methane, isoprene, and other volatile organic compounds (VOCs). The major sink of CO is the reaction with hydroxyl radical OH. The monthly net loss term was -8, -2, and 7 kt CO day⁻¹ for July, August, and September 2000, respectively (Table 1).

The fourth term is the sum of CO emission from fossil fuel and biofuel. This term varies little seasonally. From the results of the GEOS-CHEM model (Bey et al., 2001), the emissions from fossil fuel and biofuel were 31 and 0.6 kt CO day⁻¹, respectively, for the study area during the study period in year 2000.

Using the above data, the CO emission from the fires is obtained (Eq. (1)) and is compared with the number of contemporaneous hotspots in Fig. 8. The emission appears to be predominantly related to the number of hotspots during the fire events. The correlation between CO emission and hotspots becomes closer than that between mean CO abundance and hotspots in Fig. 5 for the period of late July and early August, after removal of the CO transported into the study area. Overall, the correlation coefficient (R)

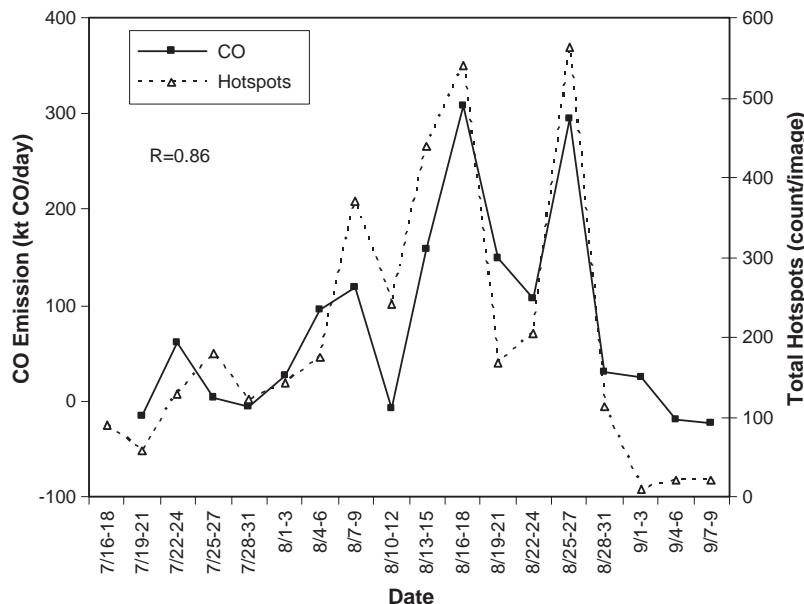


Fig. 8. Temporal variation of CO emission estimated from MOPITT data with a one-box model (Eq. (1)) versus total number of hotspots.

between CO emission and hotspots increases to 0.86 from 0.75 in Fig. 5.

Because no in-situ measurements are available, it is not possible to assess the actual CO emission from these fires estimated with the MOPITT data. Therefore, the estimate is compared with other approaches and earlier studies. Using a “bottom-up” approach (Seiler & Crutzen, 1980), the CO emission is estimated from ground information on burnt area, biomass density, and emission ratio, i.e.,

$$CO_{\text{fire}} = \sum_{\text{Image}} A(x,y)B(x,y)\beta(x,y)F_{\text{co}}(x,y) \quad (4)$$

where A is the burnt area (m^2), B is the above-ground biomass density in the burnt area ($(\text{kg dry matter}) \text{m}^{-2}$), β is the burning efficiency of the above-ground biomass, i.e., the fraction of above-ground biomass that is burnt (dimensionless), and F_{co} is the emission factor ($\text{g CO (kg dry matter)}^{-1}$) that varies with vegetation type and ecosystem. Ideally, all the parameters in Eq. (4) should vary spatially. The burnt area and the burning efficiency are the most uncertain parameters (Seiler & Crutzen, 1980). The mean emission factor (F_{co}) for extratropical forest is around $100 \text{ g CO (kg dry matter)}^{-1}$, ranging from 44 to $158 \text{ g CO (kg dry matter)}^{-1}$ (e.g., Andreae & Merlet, 2001; Duncan et al., 2003). The burning efficiency (β) is in the range of 0.2 – 0.5 for forest (Kauffman & Uhl, 1990; Seiler & Crutzen, 1980; Ward et al., 1992). Some studies used a fixed conversion factor for CO emission from a unit surface area that combines B , β , and F_{co} into one, e.g., $0.425 \text{ kg CO m}^{-2}$ for North America (Lamarque et al., 2003; Wotawa & Trainer, 2000).

In this study, the burnt area is assessed explicitly (spatially explicitly) and statistically (spatially implicitly, see Section 3.5). For the spatially explicit burned area, three scenarios are treated. The first and second use a burning efficiency of 0.3 and 0.5 , respectively, with a mean emission

factor of $107 \text{ g CO (kg dry matter)}^{-1}$ (Andreae & Merlet, 2001) and spatially explicit biomass density data (see Section 3.6) (Lines 1, 2 in Table 2). The third uses a constant conversion factor of $0.425 \text{ kg CO m}^{-2}$ (Line 3 in Table 2). For the spatially implicit burnt area, a conversion factor of $0.425 \text{ kg CO m}^{-2}$ is applied for forest (Lines 4, 5) and all landcover (Lines 6, 7), respectively. The conversion factor of $0.425 \text{ kg CO m}^{-2}$ and mean emission factor (F_{co}) of $107 \text{ g CO (kg dry matter)}^{-1}$ are for forest land cover (Andreae & Merlet, 2001; Wotawa & Trainer, 2000) and may be higher for other vegetation cover types. Finally, the CO emission from these estimates is compared with that from MOPITT data for the study area in August 2000 (Table 2).

It should be noted that due to different sources for the burnt area, the comparison in Table 2 does not match with MOPITT-based emission exactly in space and time. The only exact comparison is with Van der Werf et al. (2003) (Line 8). The spatially explicit burnt polygons (Lines 1–3) are within the same area as MOPITT data, i. e., the study area, but for year 2000 fire season, while the statistics on burnt area (Lines 4–7) are for the same period, i.e., August 2000, but for the regions described in Section 3.5. About 90% of the burnt area and total number of hotspots in the study area were located in the Northern Rockies and East Great Basin defined as the “two regions” (Lines 4 and 6) in the Table 2 (see Section 3.5). The study of Lamarque et al. (2003) (Line 9) covers the same period but for all western states of USA. Another difference is that MOPITT-based estimate provides a lower bound on CO emission while the bottom-up approach provides the total emission.

The statistics and spatially explicit data on burnt area look comparable (Table 2). The total burnt area from fire polygons was 6937 km^2 in year 2000. The statistics for the burnt forest area in the two regions of Northern Rockies and

Table 2

MOPITT-based estimate of total CO emission from the study area ($2.65 \times 10^6 \text{ km}^2$) in August 2000 in comparison with those from ground data and with earlier studies

Study/Treatment	ΣA^* (km^2)	$B\beta F_{\text{co}}^*$ (kg CO m^{-2})	β^* (–)	Emission (Mt CO)	Period (yyyy/mm)
<i>This study, Top-down Approach</i>					
MOPITT				3.87	2000/08
<i>This study, Bottom-up Approach</i>					
1 Spatially explicit burnt polygons	6937		0.3	1.30	2000
2 Spatially explicit burnt polygons	6937		0.5	2.17	2000
3 Spatially explicit burnt polygons	6937	0.425		2.95	2000
4 Statistics (Forest, the two regions)	5569	0.425		2.37	2000/08
5 Statistics (Forest, the four regions)	5642	0.425		2.40	2000/08
6 Statistics (All, the two regions)	7525	0.425		3.20	2000/08
7 Statistics (All, the four regions)	9542	0.425		4.06	2000/08
<i>Earlier studies, Bottom-up Approach</i>					
8 Van der Werf et al. (2003)	11837			6.66	2000/08
9 Lamarque et al. (2003)**	21176	0.425		9	2000/08

* B is the above-ground biomass density ($(\text{kg dry matter}) \text{m}^{-2}$); β is the burning efficiency; and F_{co} is the emission factor ($\text{g CO (kg dry matter)}^{-1}$); ΣA is the total burnt area.

** The area in Lamarque et al. (2003) covers all the western states in the United States, which is larger than the area in this study.

East Great Basin were 5569 km² for August and 6810 km² for year 2000, indicating 82% of the burning occurred in August. The statistics for total burnt area in the “two regions” was 7525 km² for August 2000, of which forest burnt area (=5569 km²) was 75%. The study area also covers part of Canada, but this was neglected because only 1.5% of the total number of hotspots in the study area was in Canada in August 2000.

On the basis of the ground-reported burnt area, the CO emission was estimated to range from 1.3 to 3 Mt CO for August 2000. Using the spatially explicit data of burnt area and biomass density, along with a mean emission factor for this region, results in a lower estimate of CO emission than that with a constant conversion factor of 0.425 kt CO km⁻² (Lines 1, 2 versus Line 3). Overall, the MOPITT-based estimate is 10%–50% larger than the bottom-up results (The emission estimates in Lines 1–3, 5 and 7 should be even lower for August 2000 or for the study area). This suggests that higher emission factors and/or burning efficiency than the mean values reported in literature may be appropriate. Another quantitative study with an inversion method also found that a MOPITT-based estimate is higher than the documented CO emission of biomass burning using the bottom-up approach for North and Central America (Arellano et al., 2004).

In Table 2, the results from two earlier studies are also shown. Van der Werf et al. (2003) estimated that 6.66 Mt CO was emitted from the study area during August 2000 with a bottom-up approach that combines satellite fire count data, country-level fire statistics, and a biogeochemical model. The MOPITT-based emission is somewhat lower (~40%) in value. The difference would be reduced if an allowance were made for the lack of sensitivity of MOPITT measurement in the boundary layer. For a larger area covering all western states of USA, Lamarque et al. (2003) concluded an emission from fires of ~9 Mt CO in August 2000, using a constant conversion factor of 0.425 kt CO km⁻² and AVHRR fire count data.

A large discrepancy is found between the ground-reported burnt area and those derived from satellite in the two earlier studies. From Van der Werf et al. (2003), the burnt area was 11415 km² for the study area in August 2000, which is about 30%–40% higher than the ground data (Table 2). For the entire USA in August 2000, the ground reported burnt area from the National Interagency Coordination Center is 11837 km². From Lamarque et al. (2003)'s numbers, the burnt area can be derived as 21176 km², which is larger than the ground data for the entire USA in August 2000.

This discrepancy of burnt area between the ground-reported data and two earlier studies with satellite data appears to be the main explanation for the difference in CO emission estimates between these two methodologies that both use a bottom-up approach (Table 2, Lines 1–7 versus Lines 8–9). We have more confidence in the ground data because: 1) Li et al. (2003) reported an estimate of 6369 km²,

which is comparable to the ground data for the region, using the HANDS method (Hot spot and NDVI Differencing Synergy, Fraser et al., 2000); 2) By overlaying AVHRR hotspot data day by day, we obtained 7063 pixels (1hotspot ≈ 1 km²) labeled as burnt for August 2000. The overlaying partly reduces the overestimate of burnt area using the total number of hotspots. The pixels labeled as burnt cover 94% of the statistical burnt area for the two regions in Table 2. The close agreement suggests that, overall, the overestimate of burnt area by fire counts is partly offset by the underestimate due to small fires, short-lived fires, and clouds.

We further examined the spatial difference in burnt area between the two spatially explicit data, the ground-reported data and that from Van der Werf et al. (2003). Transferring both data to the same grid size of 1°, we identified 26 pixels labeled as burnt in both datasets. The relationship in burnt area between the two data sets is $AREA_{ground} = 1.31 \times AREA_{van\ der\ Werf+203}$ (in km²), with a correlation coefficient of 0.61. This suggests that the two datasets are relatively similar in spatial pattern and the estimate by Van der Werf et al. (2003) appears, on average, 30% higher than the ground data. There is 1 pixel labeled as burnt in Van der Werf et al. (2003) but not in ground data, whereas 62 pixels are identified as burnt in ground data but not in Van der Werf et al., among which 41 pixels (67% of 62) are with burnt area less than 20 km² in ground data.

The possible errors in the MOPITT-based estimate in Table 2 arise from the bias in estimating each term in Eq. (1). The responsible data/procedures include CO data in the 1st and the 2nd terms, wind data in the 2nd term, gap filling in the 1st and the 2nd terms, and chemical modeling in the 3rd and the 4th terms. The mean MOPITT instrument and retrieval errors are about 10% (Emmons et al., 2004). The difference between the CO with and without gap filling, averaged for all the composites, is -1%, with a range from -7% to 4%. For wind data error estimation, comparisons were made among models and among different operation systems (Kalnay et al., 1996). For the northern hemisphere, the monthly rms (root mean square) difference in both horizontal wind components is less than 1.0 m s⁻¹ at 850 hPa, and 1.2 m s⁻¹ at 200 hPa (Kalnay et al., 1996). The CO emission by the chemical modeling is in agreement with the IPCC (1994) recommendation but 10%–20% lower than that from other global models (Bey et al., 2001). Taking the maximum errors in all the data/procedures and recalculating the CO emission with Eq. (1), the overall error for the estimate in Table 2 is found to be less than 40%, based on sensitivity analysis of the different terms.

For the bottom-up approach, uncertainties are associated with every parameter in Eq. (4), although efforts were made to reduce them with the best data available. In Andreae and Merlet (2001), the emission factor ranges ±34% from the mean with an uncertainty about 20%–30%. The discrepancies in burnt area, emission factor (F), the conversion factor (combining B , β , and F), and burning efficiency for

CO or other atmospheric gases among different studies are commonly recognized problems with the bottom-up approach (Ahern et al., 2001; Levine, 1996).

It should also be recognized that fires are a diverse phenomenon and all methods of determining their magnitude are fraught with uncertainty.

4.4. Strengths and limitations of MOPITT data for studying fire emission

The advantages of MOPITT CO data for studying fire emissions include: 1) with frequent measurement (~10 times per month) and large area coverage, temporal and spatial variations of CO emission can be examined; 2) CO emission can be directly estimated with no requirement for surface data, such as burnt area and biomass density, which are traditionally used for indirect derivation of the emission; 3) MOPITT CO data can provide an independent constraint for estimating fire emission to complement other approaches. It can reveal the non-linearity of fire emission with fuel consumption, since other factors, such as the fire phase (flaming or smoldering), also affect the CO emission level.

While MOPITT can reliably detect the CO emission from large forest fires, a quantitative analysis must consider the fact that MOPITT has a low sensitivity to the CO in the boundary layer and so the estimated CO emission may only be a lower bound. With a revisit time of 2–3 days, MOPITT suffers from discontinuous spatial coverage at a given time. Some fires can be missed completely if the fire is not large enough and/or the burning time not closely matched with the MOPITT overpass time. Another limitation is missing data resulting from the presence of clouds. This is a problem for all optical satellite instruments.

5. Conclusions

This study has enhanced our knowledge on MOPITT detection of CO emission from forest fires in three aspects: 1) CO detection in relation to the fire location and density, 2) temporal correlation between fire hotspots and atmospheric CO enhancement detected by MOPITT, and 3) methods for quantitative assessment of fire CO emission based on MOPITT data. These new findings have further demonstrated the power of this space instrument for assessing a complicated surface process.

As demonstrated with a case study in North America, MOPITT can successfully detect CO emission from large forest fires. In Fig. 3, CO and hotspot images are overlaid, and the relationship between CO emission and density and location of fires is closely examined in a zoom-in window at daily time steps. The spatial CO patterns during the fire events are found to match remarkably well with the location and density of hotspots detected by the AVHRR sensor and the wind direction in the NCEP/NCAR Reanalysis dataset.

Figs. 5 and 8 show, for the first time, that the temporal variation of CO emission from forest fires can be captured by MOPITT in 3-day composites.

This may be the first attempt to compare MOPITT assessment with forest fire CO emission estimates using ground data with a bottom-up approach. Efforts are made to collect and process best data available from ground measurement on burnt area and biomass density. Despite its low sensitivity to the boundary layer, MOPITT data result in a higher emission estimate than those using ground data. In August 2000 when large fires occurred in the study area (2.65×10^6 km²), the MOPITT-based estimate is about 4 Mt CO, in comparison with 1–3 Mt CO from the bottom-up approach for different emission factors and burnt area data (Table 2). This suggests that higher emission factors and/or higher burning efficiency than the mean values reported in literature are more appropriate since we have confidence in data of the burnt area and biomass density.

Limitations of MOPITT data include its low sensitivity to the boundary layer CO and discontinuous spatial coverage at a given time. Nevertheless, MOPITT provides a valuable CO dataset for biomass burning research in many aspects. In the future, we shall study the contribution of biomass burning to the annual CO cycle and continental/intercontinental transport of CO emitted from fires and the associated influence to local environments.

Acknowledgments

We gratefully acknowledge the following individuals and groups for their help with various data: the MOPITT team at NCAR and University of Toronto for CO data; Zhanqing Li (now at University of Maryland), Robert Fraser, Ji-zhong Jin (now at Canadian Forest Service), and Josef Cihlar of CCRS for AVHRR fire data; and Sharon Woudenberg and Warren Cohen of USDA Forest Service for biomass information; Zhanqing Li and Wei Min Hao of USDA Forest Service for ground-based burnt area data; Guido van der Werf of NASA Goddard Space Flight Center at Greenbelt and James Randerson of University of California at Irvine, for the CO emission and the related burnt area data from their studies. We are especially indebted to Zhanqing Li, Ji-zhong Jin, Dylan Jones of University of Toronto, and Doug McRae of Canadian Forest Service for their help. We are grateful to two anonymous reviewers for their constructive comments and to John McConnell of York University and Jay Kar of University of Toronto for their careful reviews and valuable comments on an earlier manuscript of this paper. The MOPITT project and this study are funded by the Natural Sciences and Engineering Research Council (NSERC) of Canada and the Canadian Space Agency (CSA). The NCAR MOPITT Team was supported by NASA's EOS Program.

References

- Ahern, F. J., Goldammer, J. G., & Justice, C. O. (Eds.) (2001). *Global and Regional Vegetation File Monitoring from Space: Planning a Coordinated International Effort*. The Hague, The Netherlands: SPB Academic Publishing bv.
- Amiro, B. D., Todd, J. B., Wotton, B. M., Logan, K. A., Flannigan, M. D., Stocks, B. J., et al. (2001). Direct carbon emissions from Canadian forest fires, 1959 to 1999. *Canadian Journal of Forest Research*, *31*, 512–525.
- Andreae, M. O., & Merlet, P. (2001). Emission of trace gases and aerosols from biomass burning. *Global Biogeochemical Cycles*, *15*, 955–966.
- Arellano, A. F., Kasibhatla, P. S., Giglio, L., van der Werf, G. R., & Randerson, J. T. (2004). Top down estimates of global CO sources using MOPITT measurements. *Geophysical Research Letters*, *31*, L01104.
- Barbosa, P. M., Stroppiana, D., Grégoire, J., & Pereira, J. M. C. (1999). An assessment of vegetation fire in Africa (1981–1991): Burned areas, burned biomass and atmospheric emissions. *Global Biogeochemical Cycles*, *13*, 933–950.
- Bergamaschi, P., Hein, R., Heimann, M., & Crutzen, P. J. (2000). Inversion modeling of the global CO cycle: 1. Inversion of CO mixing ratios. *Journal of Geophysical Research*, *105*(D2), 1909–1927.
- Bey, I., Jacob, D. J., Yantosca, R. M., Logan, J. A., Field, B. D., Fiore, A. M., et al. (2001). Global modeling of tropospheric chemistry with assimilated meteorology: Model description and evaluation. *Journal of Geophysical Research*, *106*, 23073–23095.
- Bremer, H., Kar, J., Drummond, J. R., Nichitui, F., Zou, J., Liu, J., et al. (2004). The spatial and temporal variation of MOPITT CO in Africa and South America: A comparison with SHADOZ ozone and MODIS aerosol. *Journal of Geophysical Research*, *109*, D12304.
- Cahoon Jr., D. R., Stocks, B. J., Levine, J. S., Cofer III, W. R., & Pierson, J. M. (1994). Satellite analysis of the severe 1987 forest fires in northern China and southeastern Siberia. *Journal of Geophysical Research*, *99*, 18627–18638.
- Connors, V. S., Flood, M. F., Jones, T., Gormsen, B., Nolf, S., & Reichle Jr., H. G. (1996). Global distribution of biomass burning and carbon monoxide in the middle troposphere during early April and October 1994. In J. S. Levine (Ed.), *Biomass Burning and Global Change* (pp. 835–836). Cambridge: The MIT Press.
- Cooke, W. F., Koffi, B., & Grégoire, J. -M. (1996). Seasonality of vegetation fires in Africa from remote sensing data and application to a global chemistry model. *Journal of Geophysical Research*, *101*, 21001–21065.
- Crawford, J., Olson, J., Davis, D., Chen, G., Barrich, J., Shetter, R., et al. (2003). Clouds and trace gas distributions during TRACE-P. *Journal of Geophysical Research*, *108*(D21), 8818.
- Deeter, M. N., Emmons, L. K., Francis, G. L., Edwards, D. P., Gille, J. C., Warner, J. X., et al. (2003). Operational carbon monoxide retrieval algorithm and selected results for the MOPITT instrument. *Journal of Geophysical Research*, *108*(D14), 4399.
- Deeter, M. N., et al. (2003). Operational carbon monoxide retrieval algorithm and selected results for the MOPITT instrument. *Journal of Geophysical Research*, *108*(D14), 4399.
- Deeter, M. N., Emmons, L. K., Edwards, D. P., Gille, J. C., & Drummond, J. R. (2004). Vertical resolution and information content of CO profiles retrieved by MOPITT. *Geophysical Research Letters*, *31*, L15112.
- Delmas, R. A., Loudjani, P., Podaire, A., & Menaut, J. -C. (1991). Biomass burning in Africa: An assessment of annually burned biomass. In Joel S. Levine (Ed.), *The Global Impact of Biomass Burning: Atmospheric, Climatic, and Biospheric Implications* (pp. 126–132). Cambridge: The MIT Press.
- Drummond, J. R. (1992). Measurements of Pollution in the Troposphere (MOPITT). In J. C. Gille, & G. Visconti (Eds.), *The Use of EOS for Studies of Atmospheric Physics* (pp. 77–101). New York: North-Holland.
- Drummond, J. R., & Mand, G. S. (1996). The measurements of pollution in the troposphere (MOPITT) instrument: Overall performance and calibration requirements. *Journal of Atmospheric and Oceanic Technology*, *13*, 314.
- Duncan, B. N., Martin, R. V., Staudt, A. C., Yevich, R., & Logan, J. A. (2003). Interannual and seasonal variability of biomass burning emissions constrained by satellite observations. *Journal of Geophysical Research*, *108*.
- Dwyer, E., Pinnock, S., Grégoire, J. -M., & Pereira, J. M. C. (2000). Global spatial and temporal distribution of vegetation fire as determined from satellite observations. *International Journal of Remote Sensing*, *21*, 1289–1302.
- Edwards, D. P., Halvorson, C. M., & Gille, J. C. (1999). Radiative transfer modeling for the EOS Terra satellite Measurement of Pollution in the Troposphere (MOPITT) instrument. *Journal of Geophysical Research*, *104*, 16755–16775.
- Edwards, D. P., Lamarque, J. -F., Attie, J. -L., Emmons, L. K., Richter, A., Cammas, J. -P., et al. (2003). Tropospheric ozone over the tropical Atlantic: A satellite perspective. *Journal of Geophysical Research*, *108*(D8), 4237.
- Emmons, L. K., Deeter, M. N., Gille, J. C., Edwards, D. P., Attié, J. -L., Warner, J., et al. (2004). Validation of Measurements of Pollution in the Troposphere (MOPITT) CO retrievals with aircraft in situ profiles. *Journal of Geophysical Research*, *109*(D3), D03309.
- Fraser, R. H., Li, Z., & Cihlar, J. (2000). Hotspots and NDVI differencing synergy (HANDS): A new technique for burned area mapping over boreal forest. *Remote Sensing of Environment*, *74*, 362–376.
- Giglio, L., Kendall, J. D., & Justice, C. O. (1999). Evaluation of global fire detection algorithms using simulated AVHRR infrared data. *International Journal of Remote Sensing*, *20*, 1947–1985.
- Hao, W. M., & Liu, M. -H. (1994). Spatial and temporal distribution of tropical biomass burning. *Global Biogeochemical Cycles*, *8*, 495–503.
- Heald, C. L., Jacob, D. J., Palmer, P. I., Evans, M. J., Sachse, G. W., Singh, H. B., et al. (2003). Biomass burning emission inventory with daily resolution: Application to aircraft observations of Asian outflow. *Journal of Geophysical Research*, *108*(D21), 8811.
- Hsu, N. C., Herman, J. R., Bhartia, P. K., Seftor, C. J., Torres, O., Thompson, A. M., et al. (1996). Detection of biomass burning smoke from TOMS measurements. *Geophysical Research Letters*, *23*, 745–748.
- Intergovernmental Panel on Climate Change (IPCC). (1995). Radiative forcing of climate change and an evaluation of the IPCC IS92 emission scenarios. In J. T., Houghton, et al., (Ed.), *Climate Change 1994: The Science of Climate Change*. New York: Cambridge University Press.
- Jacob, D. (1999). *Introduction to Atmospheric Chemistry*. Princeton, New Jersey: Princeton University Press.
- Jacob, D. J., Crawford, J., Kleb, M. M., Connors, V. S., Bendura, R. J., Raper, J. L., et al. (2003). Transport and chemical evolution over the Pacific (TRACE-P) mission: Design, execution, and first results. *Journal of Geophysical Research*, *108*(D20), 9000.
- Jost, H., et al. (2004). In situ observations of mid-latitude forest fire plumes deep in the stratosphere. *Geophysical Research Letters*.
- Kalnay, E., Kanamitsu, M., Kistler, R., Collins, W., Deaven, D., Gandin, L., et al. (1996). The NCEP/NCAR 40-year reanalysis project. *Bulletin of the American Meteorological Society*, *77*, 437–471.
- Kar, J., Bremer, H., Drummond, J. R., Rochon, Y. J., Jones, D., Nichitui, F., et al. (2004). Evidence of vertical transport of carbon monoxide from measurements of pollution in the troposphere (MOPITT). *Geophysical Research Letters*, *31*(23), L23105.
- Kasibhatla, P., Arellano, A., Logan, J. A., Palmer, P. I., & Novelli, P. (2002). Top-down estimate of a large source of atmospheric carbon monoxide associated with fuel combustion in Asia. *Geophysical Research Letters*, *29*(19), 1900.
- Kasischke, E. S., & French, N. H. (1995). Locating and estimating the areal extent of wildfires in Alaskan boreal forests using multiple-season AVHRR NDVI composite data. *Remote Sensing of Environment*, *51*, 263–275.

- Kauffman, J. B., & Uhl, C. (1990). Interactions of anthropogenic activities, fire, and rain forests in the Amazon basin. In J. G. Goldammer (Ed.), *Fire in the Tropical Biota. Ecological Studies*, vol. 84 (pp. 117–134). New York: Springer-Verlag.
- Khalil, M. A. K., Pinto, J. P., & Shearer, M. J. (1999). Atmospheric carbon monoxide. *Chemosphere: Global Change Science*, 1, ix–xi.
- Kittel, T. G. F., Rosenbloom, N. A., Painter, T. H., Schimel, D. S., Fisher, H. H., Grimsdell, A., et al. (1996). *The VEMAP Phase I Database: An Integrated Input Dataset for Ecosystem and Vegetation Modeling for the Conterminous United States*. <http://www.cgd.ucar.edu/vemap/>
- Lamarque, J. -F., Edwards, D. F., Emmons, L. K., Gille, J. C., Wilhelmi, O., Gerbig, C., et al. (2003). Identification of CO plumes from MOPITT data: Application to the August 2000 Idaho-Montana forest fires. *Geophysical Research Letters*, 30(13), 1688.
- Lavoué, D., Liousse, C., Cachier, H., Stocks, B. J., & Goldammer, J. G. (2000). Modeling of carbonaceous particles emitted by boreal and temperate wildfires at northern latitudes. *Journal of Geophysical Research*, 105, 26871–26890.
- Levine, J. S. (Ed.) (1991). *The Global Impact of Biomass Burning: Atmospheric, Climatic, and Biospheric Implications*. Cambridge: The MIT Press.
- Levine, J. S. (Ed.) (1996). *Biomass Burning and Global Change, vol. 1 & 2*. Cambridge: The MIT Press.
- Li, Z., Fraser, R., Jin, J., Abuelgasim, A. A., Csiszar, I., Gong, P., et al. (2003). Evaluation of algorithms for fire detection and mapping across North America from Satellite. *Journal of Geophysical Research*, 108(D2), 4076.
- Li, Z., Nadon, S., & Cihlar, J. (2000). Satellite-based detection of Canadian boreal forest fires: Development and application of the algorithm. *International Journal of Remote Sensing*, 21, 3057–3069.
- Liu, J., & Drummond, J. R. (2002, June 24–28). MOPITT detection of carbon monoxide emitted from biomass burning: A case study, proceeding at international geoscience and remote sensing symposium (IGARSS) 3 pages. *IEEE Geoscience and Remote Sensing Society Newsletter*, Toronto, Canada Toronto, Canada: IEEE Inc.
- Liu, J., Drummond, J. R., Cao, Z., Zou, J., Bremer, H., Kar, J., et al. (2004, May 17–21). MOPITT Observation of large horizontal gradients of CO at the synoptic scale. *The 2004 Joint Assembly, American Geophysical Union and Canadian Geophysical Union, Montreal, Quebec, Canada*.
- Liu, J., Drummond, J. R., Nichitiu, F., & Zou, J. (2003a, December 8–12). Correlating MOPITT CO data with ATSR fire count data. *AGU (American Geophysical Union) Fall Meeting* (p. 168). San Francisco, CA, USA: American Geophysical Union.
- Liu, J., Drummond, J. R., Zou, J., & Nichitiu, F. (2003b, June 2–5). Assessment of CO emission from biomass burning in Canada and USA based on MOPITT data. *CMOS (Canadian Meteorological And Oceanographic Society) 37th Annual Congress, Ontario, Canada*.
- Manning, M. R., Brenninkmeijer, C. A. M., & Allan, W. (1997). The atmospheric carbon monoxide budget of the southern hemisphere: Implication of $^{13}\text{C}/^{12}\text{C}$ measurements. *Journal of Geophysical Research*, 102, 10673–10682.
- Natural Resources Canada. (2004). *Canadian Wildland Fire Information System* <http://cwfis.cfs.nrcan.gc.ca/>. Canadian Forest Service.
- Pan, L., Gille, J. C., Edwards, D. P., Bailey, P. L., & Rodgers, C. D. (1998). Retrieval of tropospheric carbon monoxide for the MOPITT experiment. *Journal of Geophysical Research*, 103, 32277–32290.
- Pétron, G., Granier, G. C., Khattatov, B., Yudin, V., Lamarque, J. -F., Emmons, L., et al. (2004). Monthly CO surface sources inventory based on the 2000–2001 MOPITT satellite data. *Geophysical Research Letters*, 31, L21107.
- Reichle, H. G., Connors Jr., V. S., Holland, J. A., Hypes, W. D., Wallio, H. A., Casas, J. C., et al. (1986). Middle and upper tropospheric carbon monoxide mixing ratios as measured by a satellite borne remote sensor during November 1981. *Journal of Geophysical Research*, 91, 10865–10888.
- Rogers, C. D. (2000). Inverse methods for atmospheric sounding, theory and practice. *World Scientist*. River Edge, NJ River Edge, NJ: World Scientific.
- Roy, D. P., Lewis, P. E., & Justice, C. O. (2002). Burned area mapping using multi-temporal moderate spatial resolution data—a bi-directional reflectance model-based expectation approach. *Remote Sensing of Environment*, 83, 263–286.
- Schultz, M. G. (2002). On the use of ATSR fire count data to estimate the seasonal and interannual variability of vegetation fire emissions. *Atmospheric Chemistry and Physics*, 2, 387–392.
- Seiler, W., & Crutzen, P. J. (1980). Estimates of gross and net fluxes of carbon between the biosphere and the atmosphere from biomass burning. *Climate Change*, 2, 207–247.
- Snyder, J. P. (1989). *Map projection: A working manual*. U. S. Geological Survey Professional Paper. Supt. of Dpcs. No.: I19.16:1395, U. S. Government Printing Office, Washington, D. C.
- USDA Forest Service. (2002). *Forest Inventory and Analysis Mapmaker* <http://www.ncrs.fs.fed.us/4801/fiadb/index.htm>. North Center Research Station.
- Van der Werf, G. R., Randerson, J. T., Collatz, G. J., & Giglio, L. (2003). Carbon emissions from fires in tropical and subtropical ecosystems. *Global Change Biology*, 9, 547–562.
- Ward, D. E., Susott, R. A., Kauffman, J. B., Babbitt, R. E., Cummings, D. L., Dias, B., et al. (1992). Smoke and fire characteristics for cerrado and deforestation burns in Brazil: BASE-B experiment. *Journal of Geophysical Research*, 97, 14601–14619.
- Wotawa, G., & Trainer, M. (2000). The influence of Canadian forest fires on pollutant concentrations in the United States. *Science*, 288, 324–328.